JOURNAL OF GEOPHYSICAL RESEARCH: ATMOSPHERES, VOL. 118, 3486–3494, doi:10.1002/jgrd.50339, 2013

The signature of the stratospheric Brewer-Dobson circulation in tropospheric clouds

Ying Li[1] and David W. J. Thompson[1]

Received 4 January 2013; revised 13 March 2013; accepted 15 March 2013; published 7 May 2013.

[1] The signature of the stratospheric Brewer-Dobson circulation (BDC) in tropospheric cloudiness is investigated in CloudSat and CALIPSO data from June 2006 through April 2011. During the Northern Hemisphere winter, periods of enhanced stratospheric wave driving are associated with increased cloud incidence in the tropical tropopause transition layer (TTL) juxtaposed against decreased cloud incidence in the Arctic troposphere. The results are consistent with the physical linkages between (1) the BDC and near-tropopause temperature and (2) near-tropopause temperature and upper tropospheric cloud incidence. The key finding of the work is that changes in the stratospheric circulation not only influence cloud amounts in the troposphere but also that they do so in a coupled manner that links climate variability in the Arctic and upper tropical troposphere. The results provide a pathway through which stratospheric processes influence tropospheric climate that is in addition to stratosphere/troposphere dynamical coupling.

Citation: Li, Y., and D. W. J. Thompson (2013), The signature of the stratospheric Brewer-Dobson circulation in tropospheric clouds, *J. Geophys. Res. Atmos.*, *118*, 3486–3494, doi:10.1002/jgrd.50339.

1. Introduction

[2] The stratospheric Brewer-Dobson circulation (BDC) is marked by large-scale upwelling in the tropical stratosphere and downwelling in the extratropical stratosphere [e.g., *Holton et al*., 1995]. The circulation consists of a relatively shallow cell in the lowermost stratosphere that extends from the tropics to low-middle latitudes, and a deeper cell that extends to polar latitudes [*Plumb*, 2002; *Birner and Bönisch*, 2011]. The shallow cell and its associated temperature anomalies are believed to be driven primarily by breaking equatorial planetary waves and synoptic-scale waves [*Held and Hoskins*, 1985; *Plumb and Eluszkiewicz*, 1999; *Boehm and Lee*, 2003; *Kerr-Munslow and Norton*, 2006; *Norton*, 2006; *Randel et al*., 2008; *Ryu and Lee*, 2010; *Garny et al*., 2011; *Chen and Sun*, 2011; *Grise and Thompson*, 2012; *Zhou et al*., 2012]; the deeper cell and its associated temperature anomalies are believed to be driven primarily by planetary-scale wave breaking in the extratropical stratosphere [*Haynes et al*., 1991; *Holton et al*., 1995; *Ueyama and Wallace*, 2010; *Zhou et al*., 2012; *Grise and Thompson*, 2013].

[3] The BDC has important implications for global climate. It influences temperatures and concentrations of ozone and water vapor throughout much of the global stratosphere [*Brewer*, 1949; *Dobson*, 1956; *Holton et al*., 1995; *Mote et al*., 1996; *Shepherd*, 2007]. It transports sulfate aerosols due to explosive tropical volcanic eruptions to middle and high latitudes [*Robock*, 2000]. And notably, it is predicted to increase in strength in response to anthropogenic emissions of carbon dioxide in virtually all climate change simulations [e.g., *Butchart and Scaife*, 2001; *Butchart et al*., 2006; *Li et al*., 2008; *Garcia and Randel*, 2008; *McLandress and Shepherd*, 2009; *Butchart et al*., 2010]. The purpose of this study is to demonstrate that variability in the BDC also has a significant influence on clouds at tropospheric levels in two key regions of the atmosphere: the tropical tropopause transition layer (TTL) and the Arctic troposphere.

[4] Clouds play a central role in the climate of both the TTL and Arctic troposphere. The TTL extends from roughly the level of near-zero clear-sky radiative heating in the upper tropical troposphere (∼15 km) to the lower stratosphere (∼18.5 km) [e.g., *Highwood and Hoskins*, 1998; *Fueglistaler et al*., 2009]. Clouds in this region not only impact the radiative budget of the tropics [*Liou*, 1986; *Prabhakara et al*., 1988; *Ramanathan and Collins*, 1991; *Jensen et al*., 1996; *Rosenfield et al*., 1998; *McFarquhar et al*., 2000; *Hartmann et al*., 2001; *Haladay and Stephens*, 2009] but also regulate the water vapor content and chemical balance in the global stratosphere [*Holton et al*., 1995; *Rosenfield et al*., 1998; *Jensen et al*., 2001; *Holton and Gettelman*, 2001; *Gettelman et al*., 2002]. Clouds in the Arctic troposphere play a similarly important role in the polar radiative budget [e.g., *Curry et al*., 1996; *Kay et al*., 2011] and potentially contribute to long-term changes in Arctic sea-ice [*Francis et al*., 2005; *Kay et al*., 2011; *Kay and Gettelman*, 2009].

[5] The current evidence for linkages between stratospheric dynamics and clouds in the TTL derives from two primary observations. First, field experiment data reveal linkages between the incidence of tropical stratospheric

[1]Department of Atmospheric Science, Colorado State University, Fort Collins, Colorado, USA.

Corresponding author: Y. Li, Department of Atmospheric Science, Colorado State University, Fort Collins, Colorado 80523, USA. (yingli@atmos.colostate.edu)

©2013. American Geophysical Union. All Rights Reserved.
2169-897X/13/10.1002/jgrd.50339

waves and changes in cirrus near the tropical tropopause [e.g., *Boehm and Verlinde*, 2000]. Second, the seasonal cycle of cirrus in the uppermost tropical troposphere is more closely tied to the seasonal cycle of temperatures in the lowermost stratosphere than it is to the tropospheric processes [*Zhang*, 1993; *Virts and Wallace*, 2010]. That said, the seasonal cycle of tropical tropopause temperatures is influenced by both tropospheric and stratospheric processes [*Holton et al*., 1995; *Ueyama and Wallace*, 2010; *Grise and Thompson*, 2013]. Thus, the coherence between the seasonal cycles of TTL cirrus and tropical tropopause temperatures is not necessarily indicative of a stratospheric influence on upper tropical tropospheric clouds. We are unaware of any study that has explicitly linked wave-driven variability in the BDC to the incidence of clouds in the polar troposphere.

[6] Here we provide evidence for robust linkages between the stratospheric BDC and cloud incidence in both the TTL and polar troposphere on month-to-month timescales. The analyses exploit 5 years of remotely sensed cloud incidence data derived from the merged CALIPSO/CloudSat data set. The data are described in section 2; the results are presented in section 3; conclusions are provided in section 4.

2. Data and Analysis Details

2.1. Data

[7] The cloud data used in the study are from the CloudSat and CALIPSO satellites [*Stephens et al*., 2002]. The cloud fraction data are obtained from the Level 2B Geometrical Profiling-LIDAR product (2B-GEOPROF-LIDAR; version P2R04), which combines information from the CloudSat Cloud Profiling Radar (CPR) and CALIPSO lidar. The merged CALIPSO/CloudSat data provide a more reliable estimate of TTL cirrus than the CALIPSO data alone since the radar is capable of sensing optically opaque cirrus near convection that may be missed by the lidar pulse [*Mace et al*., 2009; *Haladay and Stephens*, 2009]. The analyses here are based on roughly 5 years of CloudSat observations from June 2006 through April 2011.

[8] The results are presented in terms of "cloud incidence," which provides a quantitative estimate of the likelihood of a cloud within a given volume sensed by the satellite. The CloudSat and CALIPSO satellites orbit the Earth roughly 14.5 times per day. The CloudSat footprint is roughly 1400 m cross track and 2500 m along track, and the vertical sampling is at roughly 240 m. Cloud incidence is calculated within all 1400 × 2500 × 240 m^3 volumes sampled by the satellite and is then binned into monthly mean, zonal-mean data with spatial resolution 1.5° (latitude) × 240 m (vertical). Cloud incidence ranges from 0 to 100%: cloud incidence of, say, 50% at 20°N and 5 km altitude indicates that a cloud was observed 50% of the time within the 1.5° × 240 m region centered on 20°N and 5 km. See *Verlinden et al*. [2011] for a more detailed description of the calculation of cloud incidence and the reason of using cloud incidence rather than ice/liquid water content.

[9] Instantaneous relationships between cloud incidence and temperature are assessed using the CloudSat European Centre for Medium-Range Weather Forecasts Auxiliary (ECMWF-AUX) product. The ECMWF-AUX product is created by interpolating the ECMWF variables to the same spatial and temporal resolution as the CloudSat CPR bins [*Partain*, 2004; *Benedetti*, 2005]. Relationships between cloud incidence and the meteorology on annual and interannual timescales are assessed using the European Centre for Medium Range Weather Forecasts (ECMWF) Interim Reanalysis (ERA-Interim) [*Simmons et al*., 2007]. The ERA-Interim reanalysis is available at six-hourly increments on a 1.5° × 1.5° horizontal mesh and at 37 discrete pressure levels.

[10] Tropopause height is defined following the World Meteorological Organization (WMO) lapse rate definition [*WMO*, 1957]. That is, the tropopause is defined as the lowest level z at which (1) the lapse rate is less than 2 K km^{-1}, and (2) the average lapse rate between this level and all higher levels within 2 km does not exceed 2 K km^{-1}. Static stability is defined as $\frac{g}{\theta}\frac{\partial\theta}{\partial z}$, where g is 9.81 m s^{-2} and θ is the potential temperature. Anomalies are computed by subtracting the long-term mean annual cycle from the data.

2.2. Brewer-Dobson Circulation Index

[11] As noted in section 1, the deep, equator-pole branch of the stratospheric Brewer-Dobson circulation is driven primarily by planetary-scale wave breaking in the extratropics [*Haynes et al*., 1991; *Holton et al*., 1995; *Ueyama and Wallace*, 2010; *Zhou et al*., 2012; *Grise and Thompson*, 2013]. The net planetary wave driving in the extratropical stratosphere is proportional to the vertical flux of wave activity in the lowermost stratosphere. The vertical flux of wave activity in the lower stratosphere is, in turn, proportional to the zonal-mean meridional eddy flux of heat at 100 hPa: $[v^*T^*]_{100\ \mathrm{hPa}}$, where the brackets denote the zonal mean and asterisks denote the deviation from zonal mean. Similar indices of stratospheric wave driving have been exploited by *Waugh et al*. [1999], *Newman et al*. [2001], *Randel et al*. [2002a], *Polvani and Waugh* [2004], and *Ueyama and Wallace* [2010].

[12] The planetary wave drag due to topography-excited stationary waves is much larger in the Northern Hemisphere (NH) than it is in the Southern Hemisphere (SH), and it is very weak during summer when the lower stratospheric zonal flow is easterly [*Charney and Drazin*, 1961]. As such, the planetary-scale wave-driven BDC has largest amplitude in the NH and during boreal winter [e.g., *Yulaeva et al*., 1994; *Rosenlof*, 1995]. For this reason, we focus on the wave fluxes averaged poleward of 30°N ($[v^*T^*]_{100\ \mathrm{hPa,\ 30–90°N}}$), and regressions on the wave fluxes are centered on the months October–March. The fluxes are calculated from six-hourly instantaneous v and T and then averaged to form monthly means.

[13] The results hinge on the links between stratospheric wave driving and near-tropopause vertical motion and thus temperatures. On month-to-month timescales, stratospheric wave driving is correlated with temperatures during both the current and subsequent month, i.e., the radiative relaxation timescales in the lower stratosphere are roughly 1 month [e.g., *Newman and Rosenfield*, 1997; *Randel et al*., 2002b]. For this reason, following *Ueyama and Wallace* [2010], we define our index of the BDC as weighted average of $[v^*T^*]_{100\ \mathrm{hPa,\ 30–90°N}}$ formed from the previous and current months values. The corresponding weights are determined via an empirical fit of the $[v^*T^*]_{100\ \mathrm{hPa,\ 30–90°N}}$ time series to lower stratospheric temperature anomalies averaged between 30°S–30°N and 70–100 hPa. As noted in

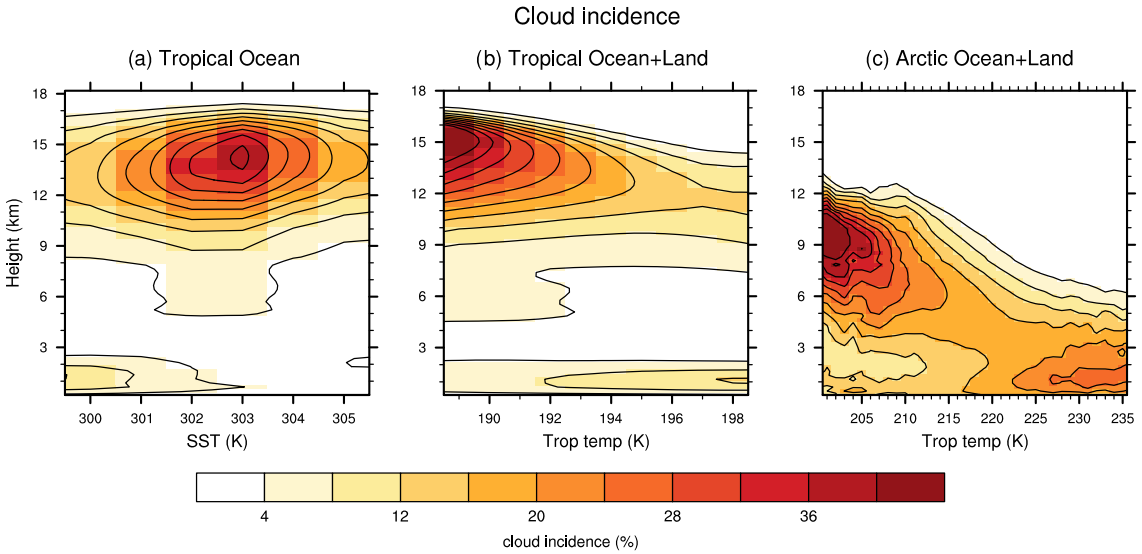

Figure 1. Cloud incidence (shading) as a function of height and (a) sea surface temperature (SST) over the tropical ocean, (b) tropopause temperature over the tropical ocean and land, and (c) tropopause temperature over the Arctic poleward of 60°N. The tropics are defined as regions equatorward of 30° within which SSTs are higher than 300 K (panel a), and tropopause temperatures are lower than 198 K (panel b). Results are based on data for all months of the year, and the seasonal cycle is not removed from the data. The bin size in all plots is 1 K. See text for details.

Ueyama and Wallace [2010], the weights applied to the previous and current months values of $[v^*T^*]_{100\ \mathrm{hPa},\ 30\text{–}90°\mathrm{N}}$ are roughly two and one, respectively. That is, the BDC index value for month i is defined as follows:

$$\mathrm{BDC}(i) = 2 \times [v^*T^*]_{100\ \mathrm{hPa},\ 30\text{–}90°\mathrm{N}}(i-1) + 1 \times [v^*T^*]_{100\ \mathrm{hPa},\ 30\text{–}90°\mathrm{N}}(i), \quad (1)$$

where (i) is the current month and $(i - 1)$ is the previous month. The results are not sensitive to the specific weights chosen in the regression for defining the BDC index, e.g., analyses based on weights ranging from 1:1 to 3:1 yield similar results. The resulting BDC index time series is then standardized so that it is dimensionless. The standardized BDC index is hereafter referred to as $\mathrm{BDC_{NH}}$. The results are not sensitive to the specific reanalysis product used to create the BDC index (the correlation coefficient between $\mathrm{BDC_{NH}}$ indices generated from the ERA-Interim and National Centers for Environmental Prediction (NCEP)/National Center for Atmospheric Research (NCAR) Reanalyses data sets is $r = 0.99$).

3. Results

[14] Variability in the large-scale BDC during NH winter influences tropopause temperatures and thus near-tropopause static stability in both the tropics [e.g., *Yulaeva et al.*, 1994; *Highwood and Hoskins*, 1998; *Gettelman and Forster*, 2002; *Birner*, 2010] and Arctic [e.g., *Birner*, 2010; *Grise et al.*, 2010]. In this section, we will first establish the robustness of the linkages between cloud incidence and tropopause temperatures in both these regions. We will then draw on the inferred linkages to motivate and support the analyses between cloud incidence and stratospheric wave driving.

3.1. Cloud Incidence as a Function of Sea Surface Temperature (SST) and Tropopause Temperature

[15] The left and middle panels in Figure 1 examine the vertical distribution of cloud incidence over the tropical ocean as a function of sea surface temperature (SST; Figure 1a) and over the tropical ocean and land as a function of tropopause temperature (Figure 1b). The tropics are defined as regions equatorward of 30° within which SSTs exceed 300 K (Figure 1a), and tropopause temperatures are less than 198 K (Figure 1b). The right panel examines the vertical distribution of cloud incidence as a function of tropopause temperatures over the Arctic poleward of 60°N (Figure 1c). The results in Figure 1 are based on contemporaneous relationships between (a) cloud incidence from CloudSat/CALIPSO product and (b) sea surface and tropopause temperatures from the ECMWF-AUX product. The seasonal cycle has not been removed from the data, and the results were calculated on a volume-by-volume basis for all satellite swaths from June 2006 through April 2011. They reflect information gleaned from more than 2×10^8 individual profile measurements over the tropics and more than 9×10^7 individual profile measurements over the Arctic. The results are not sensitive to the specific thresholds chosen to define the tropics and the Arctic.

[16] A more detailed discussion of the vertical structure of cloud incidence as a function of SST and tropopause temperature is provided in the companion paper [*Li et al.* 2013, On the linkages between cloud vertical structure and large-scale climate, to be submitted to Journal of Geophysical Research]. The key results in Figure 1 for the purpose of this study are the strong linkages between tropopause temperatures and upper tropospheric clouds at both tropical and NH polar latitudes.

[17] In the tropics, cloud incidence increases by ∼10% K^{-1} with increasing SST between 300 K to ∼303 K, and then decreases with increasing SST beyond that value (Figure 1a). The results in Figure 1a are reminiscent of those based on 1 year of CloudSat data shown in *Su et al.* [2008]. The increases in upper tropospheric cloud incidence with increasing SST are consistent with the relationships between SST and deep convection for SST above ∼300 K [e.g., *Lindzen and Nigam*, 1987; *Ramanathan and Collins*, 1991; *Waliser et al*., 1993; *Lau et al*., 1997; *Bony et al*., 1997; *Behrangi et al*., 2012]. The decreases in high level clouds beyond ∼303 K could result from increased solar radiation in the regions of subsidence that lie adjacent to the convection maximum [*Waliser and Graham*, 1993; *Waliser*, 1996; *Lau et al*., 1997; *Bony et al*., 1997; *Johnson and Xie*, 2010; *Kubar et al*., 2010].

[18] Upper tropospheric cloud incidence is also strongly linked to tropical tropopause temperatures. Cloud incidence between ∼12 and 17 km decreases by ∼4% K^{-1} with increasing tropopause temperature between 189 K and 198 K. The linkages between tropopause temperatures and cloud incidences are consistent with those derived from in situ observations of tropical stratospheric waves [*Boehm and Verlinde*, 2000], the seasonal cycle of TTL cirrus derived from CALIPSO observations [*Virts and Wallace*, 2010] and the deep convective TTL temperature signal based on collocated CloudSat and COSMIC data [*Paulik and Birner*, 2012].

[19] The linkages between tropopause temperatures and upper tropical tropospheric clouds (Figure 1b) are in part due to the coherence between tropopause temperatures and SSTs: regions of anomalously high SSTs are associated with enhanced deep convection which can force large-scale equatorial waves. Deep convection and the equatorial waves are linked to both TTL temperatures and cirrus [e.g., *Boehm and Lee*, 2003; *Norton*, 2006; *Virts et al*., 2010]. To test the independent relationship between tropical tropopause temperatures and cloud incidence, we show in Figure 2 the incidences of clouds between 15–18 km (top) and 10–15 km (bottom) as a function of sea surface (abscissa) and tropopause (ordinate) temperature. The 15 km level corresponds roughly to the base of TTL [e.g., *Shepherd*, 2007; *Fueglistaler et al*., 2009]. The results are focused on regions equatorward of 30° within which SSTs are higher than 300 K and tropopause temperatures are lower than 198 K.

[20] Cloud incidence between 15 and 18 km (Figure 2, top) is clearly a much stronger function of tropopause temperature than of SST. Regions with fixed SST are marked by increasing cloud incidence with decreasing tropopause temperature, whereas regions with fixed tropopause temperature exhibit very little dependence on SST. In contrast, tropical cloud incidence between 10 and 15 km (Figure 2, bottom) is a function of both tropopause and sea surface temperature. Cloud incidence increases with decreasing tropopause temperature but also exhibits a distinct peak near ∼302–303 K. The relationship between tropopause temperature and cloud incidence in the TTL (top panel) is not sensitive to the specific regions chosen to define the tropics, nor the specific altitudes chosen to define the TTL. For example, analyses based on other latitude bands (e.g., 5°S–5°N, 20°S–20°N) and other height levels (e.g., 16–17 km) yield similar results. The results in Figure 2 (top) strongly suggest that tropopause temperature plays a central role in determining cloud incidence in the upper tropical troposphere.

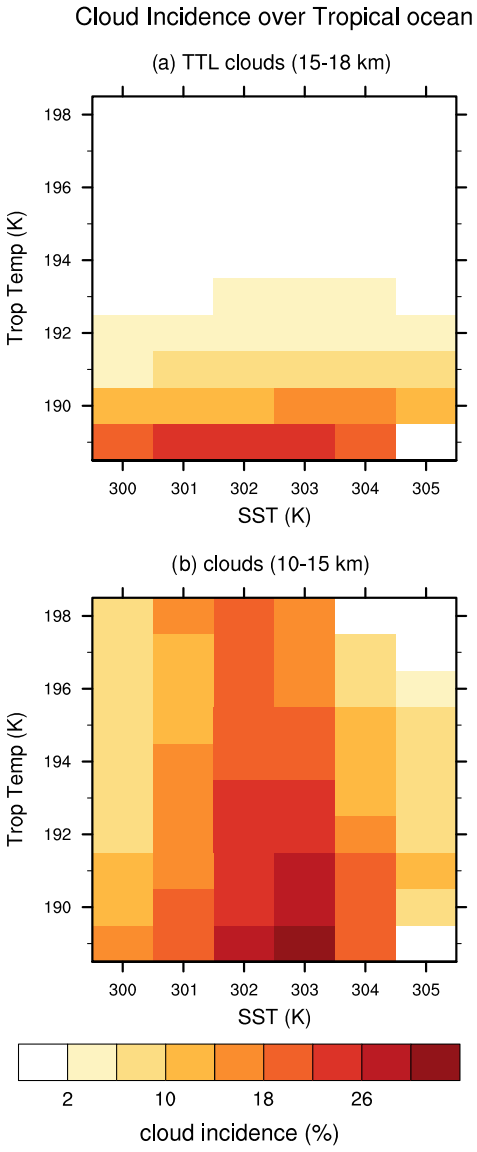

Figure 2. Cloud incidence (shading) over the tropical ocean shown as a function of SST and tropopause temperature. Results are shown for cloud incidence averaged between (a) 15–18 km and (b) 10–15 km. The tropics are defined as regions equatorward of 30° within which SSTs are higher than 300 K and tropopause temperatures are lower than 198 K. Results are based on data for all months of the year, and the seasonal cycle is not removed from the data. The bin size in all plots is 1 K. See text for details.

[21] Similar linkages between tropopause temperatures and upper tropospheric clouds are found in the Arctic. Higher tropopause temperatures correspond to depression of the tropopause and thus increased static stability (and presumably anomalous downward motion) in the upper troposphere/lower stratosphere. Such conditions are marked by a reduction in cloud incidence above ∼5 km. Upper tropospheric cloud incidence increases by ∼2% K^{-1} as tropopause temperatures decrease from ∼215 K to ∼200 K.

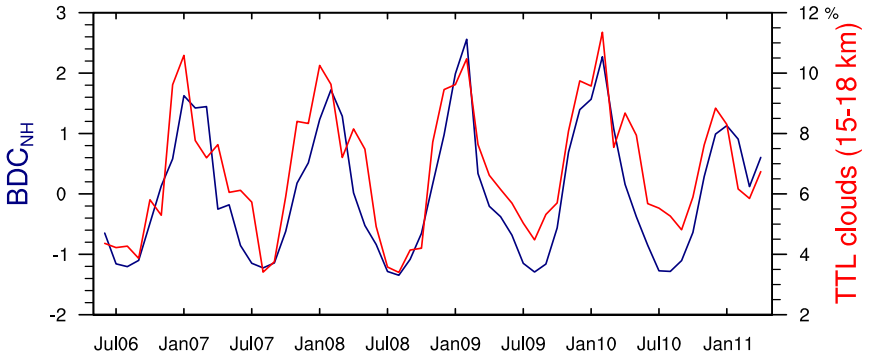

Figure 3. Monthly mean cloud incidence averaged 30°S–30°N and between 15–18 km (red; scale at right; units: %) and the standardized BDC_{NH} index (blue; scale at left). The BDC_{NH} index is based on the meridional eddy flux of heat and is defined in section 2.2.

The increases in low-level clouds for tropopause temperatures greater than ∼230 K derive from the summer season (seasonal results not shown) and are consistent with the formation of low stratiform clouds over open water in regions of large-scale subsidence.

3.2. The Signature of Brewer-Dobson Circulation in TTL Cirrus and Arctic Tropospheric Clouds

[22] In this section, we will build on the relationships between tropopause temperature and cloud incidence established in Figures 1–2 to demonstrate a robust link between the stratospheric Brewer-Dobson circulation and clouds in both the TTL and Arctic troposphere. The BDC index (BDC_{NH}) is based on the vertical flux of wave activity into the NH extratropical stratosphere during winter and is described in section 2.2.

[23] Before we examine the linkages between the BDC and tropospheric clouds on month-to-month timescales, we will first confirm the coherence between the annual cycles of NH stratospheric wave driving and cloud incidence in the TTL. The red line in Figure 3 indicates cloud incidence averaged between 30°S–30°N and 15–18 km; the blue line shows the dimensionless BDC_{NH} index. The two time series are clearly coherent: cloud incidence in the TTL and NH extratropical wave driving both peak during the boreal winter season. *Virts and Wallace* [2010] demonstrated similar coherence between TTL cirrus and tropopause temperatures in 3 years of CALIPSO data. Tropical tropopause temperatures are influenced by both equatorial planetary and extratropical waves [*Boehm and Lee*, 2003; *Kerr-Munslow and Norton*, 2006; *Norton*, 2006; *Dima and Wallace*, 2007; *Virts et al*., 2010; *Grise and Thompson*, 2013]. The coherence between cloud incidence in the TTL and extratropical planetary wave driving supports their conclusion that the large-scale BDC plays a central role in the seasonal cycle of TTL cirrus.

[24] Figures 4–5 examine the linkages between the BDC, atmospheric temperatures, and tropospheric clouds on month-to-month timescales during the NH winter months October–March. The analyses are based on anomalous data, i.e., the annual cycle has been removed from the BDC_{NH} index, atmospheric temperature, and cloud incidence. The temperature data is derived from ERA-Interim.

[25] Figure 4a shows monthly mean, zonal-mean temperature anomalies regressed on standardized wintertime values of the anomalous BDC_{NH} index. The solid black line indicates the climatological-mean (October–March) tropopause height. As noted in numerous previous studies [e.g., *Yulaeva et al*., 1994; *Rosenlof*, 1995; *Ueyama and Wallace*, 2010; *Zhou et al*., 2012; *Grise and Thompson*, 2013], periods of enhanced wave driving in the extratropical stratosphere are associated with anomalously low temperatures in the tropical lower stratosphere and anomalously high temperatures in the polar stratosphere. The negative temperature anomalies in the tropical stratosphere extend down to the tropopause level, although the amplitude of the temperature anomalies decreases below 70 hPa, consistent with the diminishing signal of extratropical planetary wave breaking in the lowermost tropical stratosphere [*Grise and Thompson*, 2013; *Ueyama et al*., 2013]. The Arctic temperature anomalies extend down to at least 400 hPa, and the static stability anomalies are statistically significant at 600 hPa. These features are consistent with the penetration of the stratospheric residual circulation to the middle troposphere in the Arctic [see also Figure 9c in *Thompson and Birner*, 2012]. The penetration of the residual circulation to the Arctic troposphere suggests that stratospheric processes may influence cloud incidence far below the polar tropopause.

[26] Figure 4b shows the corresponding changes in atmospheric static stability. Here the red and blue lines indicate the climatological-mean tropopause height plus (red) and minus (blue) the regression of tropopause height onto wintertime values of the BDC_{NH} index. Periods of enhanced stratospheric wave driving lead to (1) anomalously high tropopause heights and anomalously low static stability at ∼100 hPa in the tropics juxtaposed against (2) anomalously low tropopause heights and anomalously high static stability in the upper troposphere/lower stratosphere in the Arctic. The linkages between stratospheric wave driving and static stability near the Arctic tropopause were also shown in *Grise et al*. [2010] using GPS occultation data.

[27] Figure 4c shows the corresponding changes in cloud incidence. Month-to-month variability in stratospheric wave driving is associated with a distinct pattern of near-tropopause cloudiness. Periods of enhanced stratospheric wave driving are marked by anomalously high cloud incidence near the tropical tropopause and anomalously low cloud incidence near the Arctic tropopause. The anomalies in tropical cloud incidence are limited to the tropopause

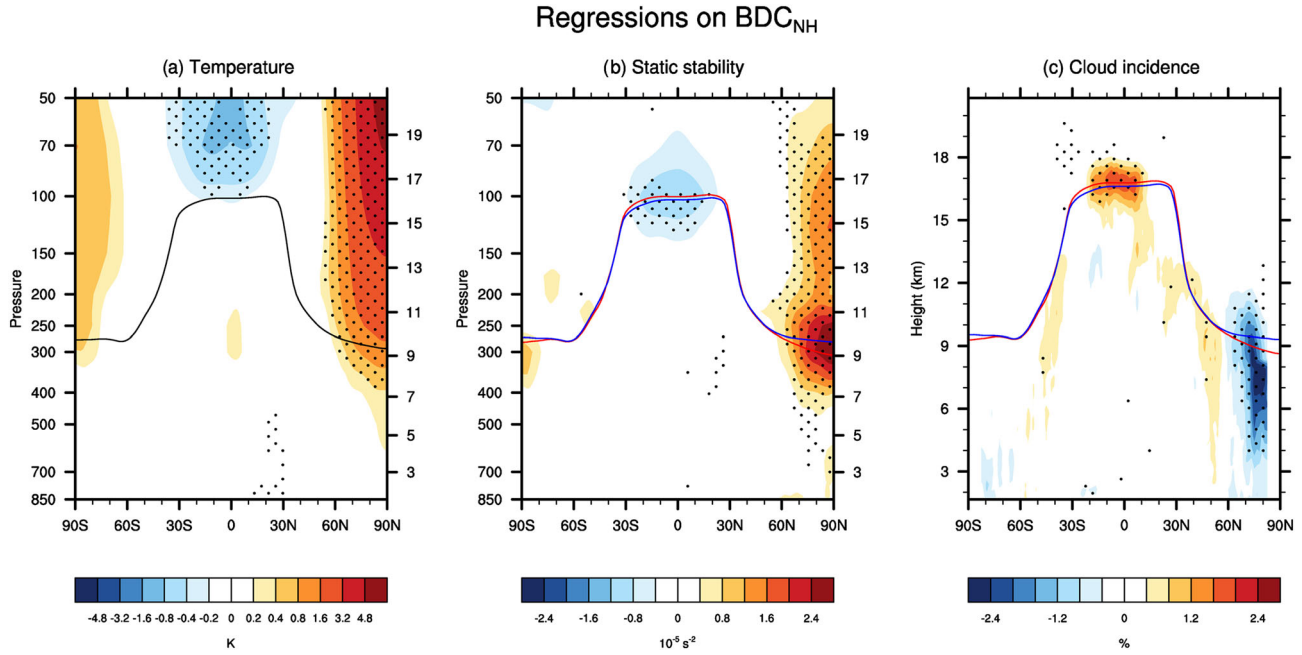

Figure 4. Regressions of zonal-mean (a) temperature, (b) static stability, and (c) cloud incidence onto standardized monthly mean values of the anomalous BDC_{NH} index. Results are shown as a function of latitude and height and are based on October–March data from June 2006 to April 2011. The seasonal cycle has been removed from the data. Units are K (temperature), 10^{-4} s^{-4} (static stability), and % (cloud incidence). The solid black line in (a) corresponds to the climatological-mean (October–March) tropopause height. The red and blue lines in (b) and (c) indicate the climatological-mean tropopause height plus and minus the regression of tropopause height onto the standardized BDC_{NH} index, respectively. The stippling indicates results that exceed 99% confidence level based on a one-tailed test of the *t*-statistic, with the effective degree of freedom computed using the criterion given in *Bretherton et al.* [1999].

region, whereas the anomalies in Arctic cloud incidence extend to the middle-upper troposphere, consistent with the penetration of the residual circulation to middle tropospheric levels there.

[28] The linkages between the BDC and cloud incidence revealed in Figure 4c are physically consistent with the relationships between (1) tropopause temperatures and cloud incidence (Figures 1 and 2), (2) the BDC and tropopause temperatures and near-tropopause static stability (Figures 4a and 4b), and (3) static stability and vertical motion. Regions of enhanced static stability near the tropopause level are associated with reduced cloud incidence, and vice versa,

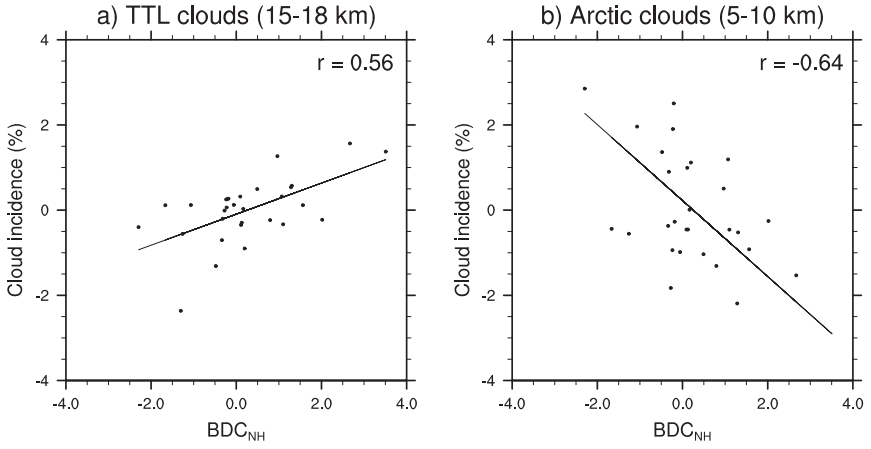

Figure 5. Scatterplots of monthly mean values of the anomalous BDC_{NH} index (abscissa) and cloud incidence (ordinate). Cloud incidence is averaged (a) equatorward of 30° and between 15–18 km and (b) poleward of 60°N and between 5 and 10 km. The solid black line denotes the least squares fit. The correlation coefficient is presented at the top right of each panel. Results are based on October–March data from June 2006 to April 2011, and the seasonal cycle has been removed from the data.

presumably through the inferred changes in vertical motion. The linkages between the BDC and cloud incidence revealed in Figure 4c are also highly significant. As shown in Figure 5, variability in the BDC accounts for more than 30% of the month-to-month variability in cloudiness in both the TTL and Arctic troposphere. The correlations are even higher (r =0.59) for TTL clouds limited to the latitude band 20°S–20°N and height levels 16–17 km (not shown). The associated correlation coefficients are significant at the 99% confidence level based on a one-tailed test of the t-statistic with an effective sampling size of 24 (using the criterion given in *Bretherton et al*. [1999]).

[29] The results presented here are based on the covariability between cloudiness and stratospheric wave driving across five boreal winter seasons. We assessed the strength of analogous relationships in association with stratospheric wave driving in the SH during the 2006–2011 period. The analysis was performed for SH spring months when the planetary wave forcing in the SH is strongest (September–December). *Eguchi and Kodera* [2007] provide anecdotal evidence of linkages between TTL cirrus and the BDC in association with the SH sudden warming of 2002. But we were unable to find a similar relationship between SH wave driving and TTL clouds during the CloudSat era, presumably because the amplitude of the wave driving in the SH is weak relative to that in the NH during the CloudSat era.

4. Concluding Remarks

[30] The planetary-scale stratospheric Brewer-Dobson circulation influences temperatures and static stability in the vicinity of the tropopause in both the tropics and Arctic. Periods of enhanced wave driving in the NH extratropical stratosphere are marked by lifting and cooling of the tropical tropopause juxtaposed against sinking and warming of the Arctic tropopause and vice versa. Here we exploited ∼5 years of data from the CloudSat and CALIPSO instruments to reveal that the influence of the BDC during NH winter extends to clouds in both the TTL and Arctic troposphere. The BDC accounts not only for the seasonal cycle in TTL cirrus (Figure 3) [*Virts and Wallace*, 2010] but also for ∼30% of the month-to-month variability in cloud incidence in both the TTL and Arctic troposphere during NH winter (Figures 4c and 5). The results reveal a novel pathway through which stratospheric processes can influence tropospheric climate.

[31] The linkages between the BDC and clouds in the TTL and Arctic troposphere are physically plausible and statistically robust. Upper tropospheric cloud incidence is linked to tropopause temperatures in both the tropics and over the Arctic (Figures 1 and 2). Tropopause temperatures and static stability in both regions are, in turn, linked to variability in the BDC (Figures 4a and 4b). The subsequent linkages between variability in the BDC and clouds in the TTL and Arctic troposphere are significant at the 99% level (Figure 5).

[32] The linkages between the BDC and clouds in the TTL and Arctic troposphere have potential implications for both climate change and the ability of models to simulate such change. Climate change simulations reveal robust increases in the strength of the BDC in response to future increases in greenhouse gases [e.g., *Butchart and Scaife*, 2001; *Butchart et al*., 2006; *Li et al*., 2008; *Garcia and Randel*, 2008; *McLandress and Shepherd*, 2009; *Butchart et al*., 2010], and at least some observations suggest that such changes have already occurred [*Thompson and Solomon*, 2009; *Hu and Fu*, 2009; *Lin et al*., 2009; *Young et al*., 2012]. The changes in cloudiness associated with a strengthening of the BDC may have notable radiative effects on both the TTL and Arctic troposphere. The radiative effects of the linkages documented here and the ability of climate models to simulate such linkages remain to be determined.

[33] **Acknowledgments.** Thanks to William J. Randel and two anonymous reviewers for their helpful comments. Thanks to Graeme L. Stephens for funding support and insightful comments. YL was funded by CloudSAT via NASA JPL and the NSF Climate Dynamics program. DWJT is funded by the NSF Climate Dynamics program.

References

Behrangi, A., T. Kubar, and B. Lambrigtsen (2012), Phenomenological description of tropical clouds using CloudSat cloud classification, *Mon. Wea. Rev.*, *140*, 3235–3249.

Benedetti, A., (2005), CloudSat AN-ECMWF ancillary data interface control document, *CloudSat Data Proc. Cent. Tech. Rep.*, Cooperative Institute for Research in the Atmosphere, Colorado State University, Fort Collins, CO, available online at http://www.cloudsat.cira.colostate.edu/ICD/AN-ECMWF/AN-ECMWF_doc_v7.pdf.

Birner, T. (2010), Residual circulation and the tropopause structure, *J. Atmos. Sci.*, *67*, 2582–2600.

Birner, T., and H. Bönisch (2011), Residual circulation trajectories and transit times into the extratropical lowermost stratosphere, *Atmos. Chem. Phys.*, *11*, 817–827.

Boehm, M. T., and S. Lee (2003), The implications of tropical Rossby waves for tropical tropopause cirrus formation and for the equatorial upwelling of the Brewer-Dobson circulation, *J. Atmos. Sci.*, *60*, 247–261.

Boehm, M. T., and J. Verlinde (2000), Stratospheric influence on upper tropospheric tropical cirrus, *Geophys. Res. Lett.*, *27*, 3209–3212, doi: 10.1029/2000GL011678.

Bony, S., K.-M. Lau, and Y. C. Sud (1997), Sea surface temperature and large-scale circulation influences on tropical greenhouse effect and cloud radiative forcing, *J. Climate*, *10*, 2055–2077.

Bretherton, C. S., M. Widmann, V. P. Dymnikov, J. M. Wallace, and I. Bladé (1999), The effective number of spatial degrees of freedom of a time-varying field, *J. Climate*, *12*, 1990–2009.

Brewer, A. W. (1949), Evidence for a world circulation provided by the measurements of helium and water vapor distribution in the stratosphere, *Quart. J. Roy. Meteor. Soc.*, *75*, 351–363.

Butchart, N., and A. A. Scaife (2001), Removal of chlorouorocarbons by increased mass exchange between the stratosphere and troposphere in a changing climate, *Nature*, *410*, 799–802.

Butchart, N., et al. (2006), Simulations of anthropogenic change in the strength of the Brewer-Dobson circulation, *Climate Dyn.*, *27*, 727–741.

Butchart, N., et al. (2010), Chemistry-climate model simulations of 21st century stratospheric climate and circulation changes, *J. Climate*, *23*, 5349–5374, doi:10.1175/2010JCLI3404.1.

Charney, J. G., and P. G. Drazin (1961), Propagation of planetary-scale disturbances from the lower into the upper atmosphere, *J. Geophys. Res.*, *66*, 83–109.

Chen, G., and L. Sun (2011), Mechanisms of the tropical upwelling branch of the Brewer-Dobson circulation: The role of extratropical waves, *J. Atmos. Sci.*, *68*, 2878–2892, doi:10.1175/JAS-D-11-044.1.

Curry, J. A., W. B. Rossow, D. Randall, and J. L. Schramm (1996), Overview of Arctic cloud and radiation characteristics, *J. Climate*, *9*, 1731–1764.

Dima, I., and J. M. Wallace (2007), Structure of the annual-mean equatorial planetary waves in the ERA-40 reanalyses, *J. Atmos. Sci.*, *64*, 2862–2880, doi:10.1175/JAS3985.1.

Dobson, G. M. B. (1956), Origin and distribution of polyatomic molecules in the atmosphere, *Proc. Roy. Soc. London*, *A236*, 187–193.

Eguchi, N., and K. Kodera (2007), Impact of the 2002, Southern Hemisphere, stratospheric warming on the tropical cirrus clouds and convective activity, *Geophys. Res. Lett.*, *34*, L05,819, doi: 10.1029/2006GL028744.

Francis, J. A., E. Hunter, J. R. Key, and X. Wang (2005), Clues to variability in Arctic minimum sea ice extent, *Geophys. Res. Lett.*, *32*, L21,501, doi: 10.1029/2005GL024376.

Fueglistaler, S., A. E. Dessler, T. J. Dunkerton, I. Folkins, Q. Fu, and P. W. Mote (2009), Tropical tropopause layer, *Rev. Geophys.*, *47*, RG1004, doi: 10.1029/2008RG000267.

Garcia, R. R., and W. J. Randel (2008), Acceleration of the Brewer-Dobson circulation due to increases in greenhouse gases, *J. Atmos. Sci.*, *65*, 2731–2739.

Garny, H., M. Dameris, W. Randel, G. E. Bodeker, and R. Deckert (2011), Dynamically forced increase of tropical upwelling in the lower stratosphere, *J. Atmos. Sci.*, *68*, 1214–1233.

Gettelman, A., and P. M. Forster (2002), A climatology of the tropical tropopause layer, *J. Meteor. Soc. Japan*, *80*, 911–924.

Gettelman, A., W. J. Randel, F. Wu, and S. T. Massie (2002), Transport of water vapor in the tropical tropopause layer, *29*, 1009, doi: 10.1029/2001GL013818.

Grise, K. M., and D. W. J. Thompson (2012), Equatorial planetary waves and their signature in atmospheric variability, *J. Atmos. Sci.*, *69*, 857–874.

Grise, K. M., and D. W. J. Thompson (2013), On the signatures of equatorial and extratropical wave forcing in tropical tropopause layer temperatures, *J. Atmos. Sci.*, *70*, 1084–1102.

Grise, K. M., D. W. J. Thompson, and T. Birner (2010), A global survey of static stability in the stratosphere and upper troposphere, *J. Climate*, *23*, 2275–2292.

Haladay, T., and G. Stephens (2009), Characteristics of tropical thin cirrus clouds deduced from joint CloudSat and CALIPSO observation, *J. Geophys. Res.*, *114*, D00A25, doi:10.1029/2008JD010675.

Hartmann, D. L., J. R. Holton, and Q. Fu (2001), The heat balance of the tropical tropopause, cirrus, and stratospheric dehydration, *Geophys. Res. Lett.*, *28*, 1969–1972.

Haynes, P. H., M. E. McIntyre, T. G. Shepherd, C. J. Marks, and K. P. Shine (1991), On the "downward control" of extratropical diabatic circulations by eddy-induced mean zonal forces, *J. Atmos. Sci.*, *48*, 651–680.

Held, I. M., and B. J. Hoskins (1985), Large-scale eddies and the general circulation of the troposphere, *Adv. Geophys.*, *28A*, 3–31.

Highwood, E. J., and B. J. Hoskins (1998), The tropical tropopause, *Quart. J. Roy. Meteor. Soc.*, *124*, 1579–1604.

Holton, J. R., and A. Gettelman (2001), Horizontal transport and the dehydration of the stratosphere, *Geophys. Res. Lett.*, *28*, 2799–2802.

Holton, J. R., P. H. Haynes, M. E. McIntyre, A. R. Douglass, R. B. Rood, and L. Pfister (1995), Stratosphere-troposphere exchange, *Rev. Geophys.*, *33*, 403–439.

Hu, Y., and Q. Fu (2009), Stratospheric warming in Southern Hemisphere high latitudes since 1979, *Atmos. Chem. Phys.*, *9*, 4329–4340, doi: 10.5194/acp-9-4329-2009.

Jensen, E., O. Toon, H. Selkirk, J. Spinhirne, and M. Schoeberl (1996), On the formation and persistence of subvisible cirrus clouds near the tropical tropopaus, *J. Geophys. Res.*, *101*, 21,361–21,375.

Jensen, E. J., L. Pfister, A. S. Ackerman, A. Tabazadeh, and O. B. Toon (2001), A conceptual model of the dehydration of air due to freezedrying by optically thin, laminar cirrus rising slowly across the tropical tropopaus, *J. Geophys. Res.*, *106*, 17,237–17,252.

Johnson, N. C., and S.-P. Xie (2010), Changes in the sea surface temperature threshold for tropical convection, *Nat. Geosci.*, *3*, 842–845.

Kay, J. E., and A. Gettelman (2009), Cloud influence on and response to seasonal Arctic sea ice loss, *J. Geophys. Res.*, *114*, D18,204, doi: 10.1029/2009JD011773.

Kay, J. E., K. Raeder, A. Gettelman, and J. Anderson (2011), The boundary layer response to recent Arctic sea ice loss and implications for high-latitude climate feedbacks, *J. Climate*, *24*, 428–447, doi: 10.1175/2010JCLI3651.1.

Kerr-Munslow, A. M., and W. A. Norton (2006), Tropical wave driving of the annual cycle in tropical tropopause temperatures. Part I: ECMWF analyses, *J. Atmos. Sci.*, *63*, 1410–1419.

Kubar, T. L., D. E. Waliser, and J. Li (2010), Boundary layer and cloud structure controls on tropical low cloud cover using A-Train satellite data and ECMWF analyses, *J. Climate*, *24*, 194–215, doi: 10.1175/2010JCLI3702.1.

Lau, K.-M., H. T. Wu, and S. Bony (1997), The role of large scale atmospheric circulation in the relationship between tropical convectio and sea surface temperature, *J. Climate*, *10*, 381–392.

Li, F., J. Austin, and R. J. Wilson (2008), The strength of the Brewer-Dobson circulation in a changing climate: Coupled chemistry-climate model simulations, *J. Climate*, *21*, 40–57.

Lin, P., Q. Fu, S. Solomon, and J. M. Wallace (2009), Temperature trend patterns in Southern Hemisphere high latitudes: Novel indicators of stratospheric change, *J. Climate*, *22*, 6325–6341.

Lindzen, R. S., and S. Nigam (1987), On the role of sea surface temperature gradients in forcing low level winds and convergence in the tropics, *J. Atmos. Sci.*, *44*, 2418–2436.

Liou, K. N. (1986), Influence of cirrus clouds on weather and climate processes: A global perspective, *Mon. Wea. Rev.*, *114*, 1167–1199.

Mace, G. G., Q. Zhang, M. Vaughn, R. Marchand, G. Stephens, C. Trepte, and D. Winker (2009), A description of hydrometeor layer occurrence statistics derived from the first year of merged CloudSat and CALIPSO data, *J. Geophys. Res.*, *114*, D00A26, doi:10.1029/2007JD009755.

McFarquhar, G. M., A. J. Heymsfield, J. Spinhirne, and B. Hart (2000), Thin and subvisual tropopause tropical cirrus: Observations and radiative impacts, *J. Atmos. Sci.*, *57*, 1841–1853.

McLandress, C., and T. G. Shepherd (2009), Simulated anthropogenic changes in the Brewer-Dobson circulation, including its extension to high latitudes, *J. Climate*, *22*, 1516–1540.

Mote, P. W. (1996), An atmospheric tape recorder: The imprint of tropical tropopause temperatures on stratospheric water vapor, *J. Geophys. Res.*, *101*, 3989–4006, doi:10.1029/95JD03422.

Newman, P. A., and J. E. Rosenfield (1997), Stratospheric thermal damping times, *Geophys. Res. Lett.*, *24*, 433–436.

Newman, P. A., E. R. Nash, and J. E. Rosenfield (2001), What controls the temperature of the Arctic stratosphere during the spring? *J. Geophys. Res.*, *106*, 19,999–20,010.

Norton, W. A. (2006), Tropical wave driving of the annual cycle in tropical tropopause temperatures. Part II: Model results, *J. Atmos. Sci.*, *63*, 1420–14,331.

Partain, P. (2004), Cloudsat ECMWF-AUX auxiliary data process description and interface control document, *CloudSat Data Proc. Cent. Tech. Rep.*, Cooperative Institute for Research in the Atmosphere, Colorado State University, Fort Collins, CO, available online at http://cloudsat.cira.colostate.edu/ICD/ECMWF-AUX/ECMWF-AUX_PDICD_3.0.pdf.

Paulik, L. C., and T. Birner (2012), Quantifying the deep convective temperature signal within the tropical tropopause layer (TTL), *Atmos. Chem. Phys.*, *12*, 12183–12195, doi:10.5194/acp-12-12183-2012.

Plumb, R. A. (2002), Stratospheric transport, *J. Meteor. Soc. Japan*, *80*, 793–809.

Plumb, R. A., and J. Eluszkiewicz (1999), The Brewer-Dobson circulation: Dynamics of the tropical upwelling, *J. Atmos. Sci.*, *56*, 868–890.

Polvani, L. M., and D. W. Waugh (2004), Upward wave activity flux as precursor to extreme stratospheric events and subsequent anomalous weather regimes, *J. Climate*, *17*, 3548–3554.

Prabhakara, C., R. S. Fraser, G. Dalu, M. L. C. Wu, R. J. Curran, and T. Styles (1988), Thin cirrus clouds: Seasonal distribution over oceans deduced from Nimbus-4 IRIS, *J. Appl. Meteor.*, *27*, 379–399.

Ramanathan, V., and W. Collins (1991), Thermodynamics regulation of ocean warming by cirrus clouds deduced from observations of the 1987, *El Niño, Nature*, *351*, 27–32.

Randel, W. J., F. Wu, and R. Stolarski (2002a), Changes in column ozone correlated with the stratosphere EP flux, *J. Meteor. Soc. Japan*, *80*, 849–862.

Randel, W. J., R. R. Garcia, and F. Wu (2002b), Time-dependent upwelling in the tropical lower stratosphere estimated from the zonal-mean momentum budget, *J. Atmos. Sci.*, *59*, 2141–2152.

Randel, W. J., R. R. Garcia, and F. Wu (2008), Dynamical balances and tropical stratospheric upwelling, *J. Atmos. Sci.*, *65*, 3584–3595.

Robock, A. (2000), Volcanic eruptions and climate, *Rev. Geophys.*, *38*, 191–219.

Rosenfield, J. E., D. B. Considine, M. R. Schoeberl, and E. V. Browell (1998), The impact of subvisible cirrus clouds near the tropical tropopause on stratospheric water vapor, *Geophys. Res. Lett.*, *25*, 1883–1886.

Rosenlof, K. H. (1995), Seasonal cycle of the residual mean meridional circulation in the stratosphere, *J. Geophys. Res.*, *100*, 5173–5191.

Ryu, J.-H., and S. Lee (2010), Effect of tropical waves on the tropical tropopause transition layer upwelling, *J. Atmos. Sci.*, *67*, 3130–3148.

Shepherd, T. G. (2007), Transport in the middle atmosphere, *J. Meteor. Soc. Japan*, *85B*, 165–191.

Simmons, A., S. Uppala, D. Dee, and S. Kobayashi (2007), ERA-Interim: New ECMWF reanalysis products from 1989 onwards, *ECMWF Newsletter*, *110*, 25–35, ECMWF , Reading, United Kingdom.

Stephens, G., et al. (2002), The CloudSat mission and the A-train: A new dimension of space-based observations of clouds and precipitation, *Bull. Amer. Meteor. Soc.*, *83*, 1771–1790, doi:10.1175/BAMS-83-12-1771.

Su, H., J. H. Jiang, D. G. Vane, and G. L. Stephens (2008), Observed vertical structure of tropical oceanic clouds sorted in large-scale regime, *Geophys. Res. Lett.*, *35*, L24,704, doi:10.1029/2008GL035888.

Thompson, D. W. J., and T. Birner (2012), On the linkages between the tropospheric isentropic slope and eddy fluxes of heat during Northern Hemisphere winter, *J. Atmos. Sci.*, *69*, 1811–1823.

Thompson, D. W. J., and S. Solomon (2009), Understanding recent stratospheric climate change, *J. Climate*, *22*, 1934–1943.

Ueyama, R., and J. M. Wallace (2010), To what extent does high-latitude wave forcing drive tropical upwelling in the Brewer-Dobson circulation? *J. Atmos. Sci*, *67*, 1232–1246.

Ueyama, R., E. P. Gerber, J. M. Wallace, and D. M. W. Frierson (2013), The role of high-latitude waves in the intraseasonal to seasonal variability of tropical upwelling in the Brewer-Dobson circulation, *J. Atmos. Sci.*, in press, doi:10.1175/JAS-D-12-0174.1.

Verlinden, K. L., D. W. J. Thompson, and G. L. Stephens (2011), The three-dimensional distribution of clouds over the Southern Hemisphere high latitudes, *J. Climate*, *24*, 5799–5811.

Virts, K. S., and J. M. Wallace (2010), Annual, interannual, and intraseasonal variability of tropical tropopause transition layer cirrus, *J. Atmos. Sci.*, *67*, 3097–3112.

Virts, K. S., J. M. Wallace, Q. Fu, and T. P. Ackerman (2010), Tropical tropopause transition layer cirrus as represented by CALIPSO lidar observation, *J. Atmos. Sci.*, *67*, 3113–3129.

Waliser, D. E. (1996), Formation and limiting mechanisms for very high sea surface temperature: Linking the dynamics and thermodynamic, *J. Climate*, *9*, 161–188.

Waliser, D. E., and N. E. Graham (1993), Convective cloud systems and warm-pool sea surface temperatures: Coupled interactions and self-regulation, *J. Geophys. Res.*, *98*, 12,881–12,893.

Waliser, D. E., N. E. Graham, and C. Gautier (1993), Comparison of the highly reflective cloud and outgoing longwave radiation datesets for use in estimating tropical deep convection, *J. Climate*, *6*, 331–353.

Waugh, D., W. Randel, S. Pawson, P. Newman, and E. Nas (1999), Persistence of the lower stratospheric polar vortices, *J. Geophys. Res.*, *104*, 27,191–27,201.

WMO (1957), Meteorology – A three-dimensional science, *WMO Bull*, *6*, 134–138.

Young, P. J., K. H. Rosenlof, S. Solomon, S. C. Sherwood, Q. Fu, and J.-F. Lamarque (2012), Changes in stratospheric temperatures and their implications for changes in the Brewer-Dobson circulation, *J. Climate*, *25*, 1759–1772, doi:10.1175/2011JCLI4048.1.

Yulaeva, E., J. Holton, and J. M. Wallace (1994), On the cause of the annual cycle in tropical lower-stratospheric temperatures, *J. Atmos. Sci.*, *51*, 169–174.

Zhang, C. (1993), On the annual cycle in highest, coldest clouds in the tropics, *J. Climate*, *6*, 1987–1990.

Zhou, T., M. A. Geller, and W. Lin (2012), An observational study on the latitudes where wave forcing drives Brewer-Dobson upwelling, *J. Atmos. Sci.*, *69*, 1916–1935.